PHOTONICS Research

Broadening and enhancing 2.7 μm emission spectra in Er/Ho co-doped oxyfluoride germanosilicate glass ceramics by imparting multiple local structures to rare earth ions

Qunhuo Liu,[1] Ying Tian,[1,*] Wenhua Tang,[1] Feifei Huang,[1] Xufeng Jing,[2] Junjie Zhang,[1] and Shiqing Xu[1,3]

[1]College of Materials Science and Engineering, China Jiliang University, Hangzhou 310018, China
[2]Institute of Optoelectronic Technology, China Jiliang University, Hangzhou 310018, China
[3]e-mail: sxucjlu@163.com
*Corresponding author: tianying0204@163.com

Received 8 December 2017; revised 5 February 2018; accepted 6 February 2018; posted 6 February 2018 (Doc. ID 314959); published 29 March 2018

Er/Ho co-doped oxyfluoride germanosilicate glass and glass ceramics are prepared and compared. The results indicate that the glass consists of SiO_4 and GeO_4 structural units, while the network of the glass ceramics consists of SiO_4, GeO_4, and GeO_6 units together with $NaYF_4$ nanocrystals. The presence of multiple local structures in glass ceramics creates a range of dipole environments, which is beneficial to the broadening of 2.7 μm emission. Two other reasons are attributed to the broadening of 2.7 μm emission in glass ceramics: the energy-level splitting of Er^{3+} and the enhancement of the Ho^{3+}:$^5I_6 \rightarrow {}^5I_7$ transition in $NaYF_4$ nanocrystals.

OCIS codes: (160.5690) Rare-earth-doped materials; (160.3380) Laser materials; (160.2750) Glass and other amorphous materials; (300.6340) Spectroscopy, infrared.

https://doi.org/10.1364/PRJ.6.000339

1. INTRODUCTION

Lasers in the mid-infrared region, covering the 2 to 5 μm wavelengths, are of great interest in scientific research and practical applications [1–3]. Specifically, broadband tunable mid-infrared lasers have widespread applications. For example, molecular species such as HF, H_2O, CO, and CO_2, have high absorption cross sections in this spectral range [4], and hence a broadband mid-infrared region laser exhibits promising applications in highly sensitive chemical analysis. Laser transitions of rare-earth (RE) cations that generate emissions in the range of 3 μm include the $^4I_{11/2} \rightarrow {}^4I_{13/2}$ transition of Er^{3+}, the $^5I_6 \rightarrow {}^5I_7$ transition of Ho^{3+}, and the $^6H_{13/2} \rightarrow {}^6H_{15/2}$ transition of Dy^{3+}.

Considerable effort has been made towards pursuing suitable host materials for the mid-infrared spectral region in recent decades. Mid-infrared emissions are readily vulnerable to multiphonon relaxation that can only be achieved in host materials with low phonon energy. To date, several glass materials have been proposed as candidates for mid-infrared fibers, including oxyfluoride glass ceramics [5], germanate [6], tellurite [7], fluoride [8], and chalcogenide glasses [4]. Here, it is worth noting that oxyfluoride glass ceramics combine the advantages of the low-phonon-energy environment of fluoride nanocrystals (NCs) and excellent macroscopic properties of an oxide glass matrix [9–11]. Therefore, they are considered efficient and promising materials for mid-infrared laser output. In our previous work [12], we demonstrated that oxyfluoride silicate glass ceramics have better mid-infrared emission properties than corresponding glass materials.

In glasses, the structure of the cationic sites is not strictly fixed and can show differences in the angle and distance bonds to the surrounding anions, which determines inhomogeneous broadening of the spectral lines [13]. Furthermore, in GeO_2- and TeO_2-based glasses in which more than one structural unit exists, a range of dipole environments are created for RE ions that are ideal for obtaining broadband spectra [14]. We [15] and others [16] have proved that silicate glass with proper GeO_2 can provide broadband emission spectra. Therefore, we expect to be able to acquire broadband emission spectra in oxyfluoride germanosilicate glass ceramics by enabling a rare-earth dopant to distribute in multiple local structures including SiO_4 tetrahedron, GeO_4 tetrahedron, and fluoride NCs, etc.

Furthermore, the partial additions of GeO_2 at the expense of SiO_2 in oxyfluoride silicate glass ceramics can decrease their maximum phonon energy and improve their refractive index, which is beneficial to attaining higher absorption and emission cross sections of mid-infrared emissions [14]. What's more, the reports involving oxyfluoride germanosilicate glass ceramics are very few, and it is interesting to investigate the complicated glass structure and corresponding mid-infrared emission properties.

In this work, a series of Er/Ho co-doped oxyfluoride germanosilicate glass and glass ceramic samples containing $NaYF_4$ NCs are prepared. The $NaYF_4$ NCs are characterized by X-ray diffraction (XRD) and transmission electron microscopy (TEM). The glass structure is investigated by Fourier-transformed infrared (FTIR) spectra. Upconversion and mid-infrared emission properties and a corresponding energy transfer mechanism in glass and glass ceramics are discussed. Additionally, the energy transfer coefficients of Er^{3+}:$^4I_{11/2}$ → Ho^{3+}:$^5I_6$ and Er^{3+}:$^4I_{13/2}$ → Ho^{3+}:$^5I_7$ are both calculated to understand the change in emission properties.

2. EXPERIMENT

Glass with composition of $25SiO_2-25GeO_2-15Al_2O_3-15Na_2O-10NaF-9.2YF_3-0.5ErF_3-0.3HoF_3$ (named SGG) was prepared by the melt-quenching method, starting from analytical-grade raw materials in powder form. The raw materials with required proportion were mixed homogeneously and put into a covered corundum crucible in order to prevent the vaporization of fluoride. Then the crucible was placed in an elevator furnace at 1450°C, where it remained for half an hour. After melting, the glass was quenched on preheated stainless steel plates before being annealed at 450°C for 2 h to release inner stress. A fraction of each sample was grinded.

Transparent oxyfluoride glass ceramics were obtained from the precursor glasses by thermal treatment method. The precursor glasses were put into an oven at 600°C, 620°C, 640°C, and 660°C (named SGGC1, SGGC2, SGGC3, and SGGC4, respectively) for 2 h. However, the SGGC4 sample became opalescent due to excessive devitrification at high temperature. Finally, the glass and the glass ceramics were cut and polished into samples with thickness of 2 mm for structural and spectroscopic property measurements.

The densities of the samples were measured by the Archimedes method, using distilled water as the immersion liquid. The differential scanning calorimeter (DSC) curve was obtained using a NETZSCH DTA 404 personal computer PC, and the heating rate of the powder sample was 10 K/min. XRD analysis of the samples was performed with Rigaku D/max2550 diffractometer using $Cu-K\alpha1$ radiation. The micrographs of the glass ceramics were measured by TEM (FEI TF20), and FTIR spectra were measured by Nicolet iS50 spectrometer from the Thermo Fisher Scientific in the range of 400–1300 cm^{-1}. Absorption spectra were measured by a PerkinElmer Lambda 900UV–vis–NIR spectrophotometer in the range of 350–1700 nm with a resolution of 1 nm. Mid-infrared emission spectra were measured by a FLS980 spectrometer from Edinburgh Instruments Ltd. and detected with a liquid-nitrogen-cooled PbS detector upon excitation by a 980 nm laser diode (LD). All the measurements were taken at room temperature and other conditions were kept as same as possible.

3. RESULTS AND DISCUSSION

A. Differential Thermal Analysis

The DSC curve of the SGG sample is represented in Fig. 1. The glass transition temperature T_g of the glass appears around 500°C. The weak exothermal peak around 620°C represents the crystallization of fluoride component of the glass matrix, while the strong exothermal peak around 736°C corresponds to the crystallization of germanosilicate oxides of the glass matrix. The heat treatment temperature was thus selected as 600°C, 620°C, 640°C, and 660°C. To prevent the RE ions from entering fluoride NCs and resulting in narrow emission spectra, the heat treatment duration cannot be too long and was 2 h in our case. The glass ceramic sample heated to 660°C was devitrified. Importantly, the thermal stability parameter $T_{x2}-T_g=201$°C (where T_{x2} represents the onset crystallization temperature corresponding to the second exothermal peak in the DSC curve) is high, which is favorable for the glass fiber drawing.

B. Morphological Characteristics

The X-ray diffraction patterns for glass and glass ceramic samples are shown in Fig. 2(a). The absence of any sharp crystallization peak in the XRD curve of the SGG sample is owing to the amorphous structural nature of glass. All XRD curves of the glass ceramic samples presented sharp characteristic peaks in the same position, corresponding to the α-$NaYF_4$ crystalline phase (JCPDS No. 060342). The results also indicate that the change of heat treatment temperature ranging from 600°C to 640°C has no obvious influence on the type of the crystalline phase in the glass ceramic. However, the diffraction peaks of samples heated to 600°C, 620°C, and 640°C are gradually stronger, indicating that the size of $NaYF_4$ crystal becomes large as the heat treatment temperature rises. The inset of Fig. 2(a) shows the prepared samples (from left: SGG, SGGC1, SGGC2, and SGGC3) in daylight. It is seen that the first three samples show high transparency, but the SGGC3 sample is a little opaque. What's more, it can be found that the diffraction peaks present a slight shift to large angle, owing to lattice contraction resulting from the partial substitution of Y^{3+} ions (radius 1.015 Å) with Er^{3+} ions of smaller radius (1.00 Å) [17].

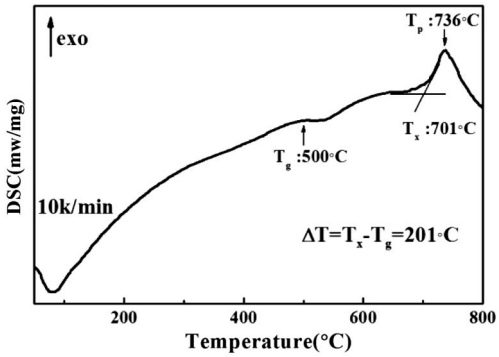

Fig. 1. DSC curve of oxyfluoride germanosilicate glass.

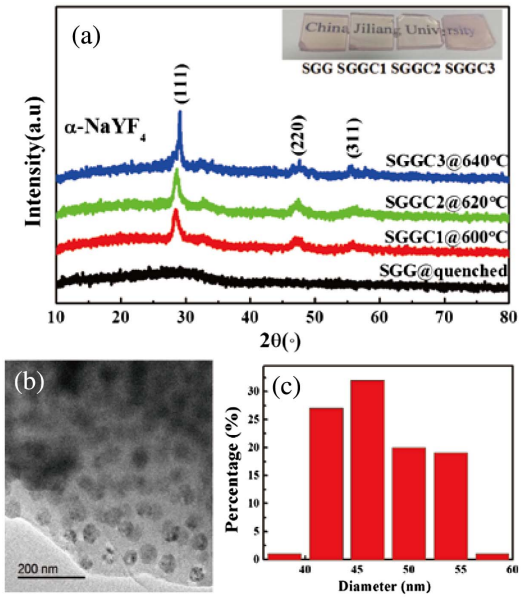

Fig. 2. (a) XRD patterns of glass and glass ceramics. (b) TEM picture of SGGC2 sample and (c) size distribution histogram of the $NaYF_4$ NCs in the SGGC2 sample.

This result is important because it indicates that the distribution of rare earth ions in glass and NCs can be controlled by altering heat treatment temperature, which is the precondition of the tuning of spectral bandwidth. To get further insight into the size, morphology, and distribution of $NaYF_4$ NCs in glass matrix, a TEM image of the SGGC2 sample is shown in Fig. 2(b). It is evident that spherical NCs, mainly sized 40–55 nm [see Fig. 2(c)], are homogenously distributed in the glass matrix.

C. Structural Analysis

The density measurement of glass and glass ceramics can give a rough macroscopic overview of the change in structural packing. The density of the SGG, SGGC1, SGGC2, and SGGC3 samples is 3.053, 3.076, 3.077, and 3.079 g/cm^{-3}, respectively. The increased density suggests a more compact glass structure in glass ceramic, which can be attributed to the structure-ordered crystallization process. Figure 3 illustrates the FTIR absorption spectra of the oxyfluoride germanosilicate glass and glass ceramics. FTIR spectroscopy is able to obtain essential information concerning the arrangement of the structural units in the glass materials. The bands at around 435 and 1000 cm^{-1} are corresponding to Si-O-Si bending vibration and asymmetric stretching, respectively [18]. The band near 880 cm^{-1} is assigned to Ge-O-Ge asymmetric stretching vibration in the GeO_4 tetrahedral unit, while the band close to 695 cm^{-1} is assigned to Ge-O-Ge stretching vibration in GeO_6 units [19,20], which was not observed in the glass sample. This suggests that the heat treatment induces some Ge^{4+} cations to incorporate in the glass ceramic network as GeO_6 units. It can be explained that the generation of bridging oxygen in glass matrix, accompanied by the crystallization of $NaYF_4$ NCs, leads to the transformation from GeO_4 to GeO_6 units. Therefore, it can be concluded that the glass network consists of SiO_4 and GeO_4 structural units while the network of the glass ceramics consists of SiO_4, GeO_4, and GeO_6 units.

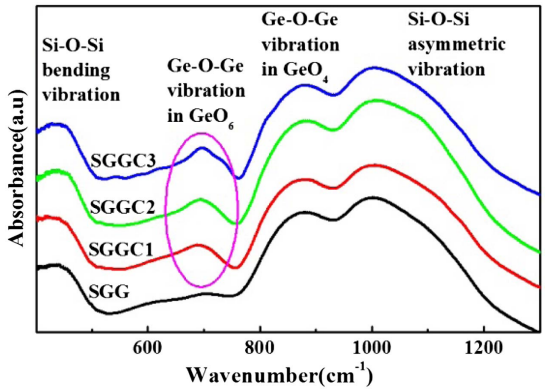

Fig. 3. FTIR absorption spectra of oxyfluoride germanosilicate glass (SGG) and glass ceramics (SGGCs).

D. Absorption Spectra

Figure 4(a) presents the absorption spectra of all prepared samples. Typical absorption bands attributed to Er^{3+} and Ho^{3+} ions' transitions from ground state to excited state levels were observed and labeled. The ultraviolet absorption cutoff wavelength of the SGGC3 sample exhibits an obvious redshift owing to the light-scattering phenomenon in the translucent SGGC3 sample. In addition, as shown in Fig. 4(b), weak Stark split peaks appear in the 1.53 μm absorption band in SGGC samples at around 1560 nm due to the crystal field effect. In the case of Er^{3+}, the transitions $^4I_{15/2} \rightarrow {}^2H_{11/2}$ and

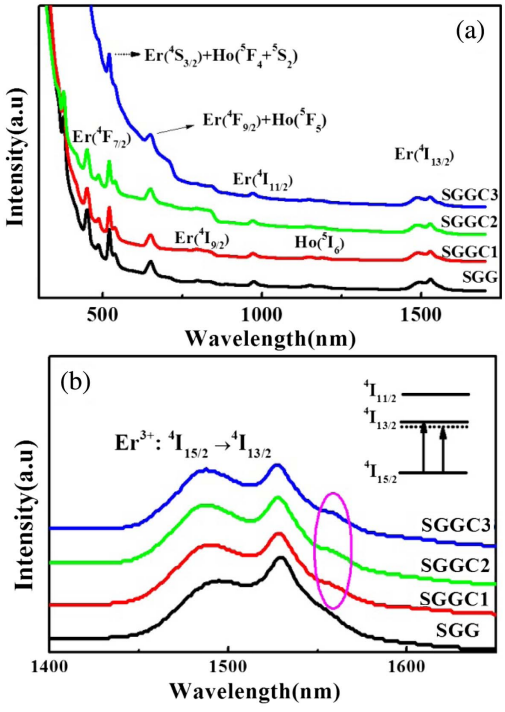

Fig. 4. Absorption spectra of glass and glass ceramic samples in the range of (a) 400–1700 nm and (b) 1400–1700 nm.

$^4I_{15/2} \rightarrow {}^4G_{11/2}$ are hypersensitive, and are sensitive to small changes of local environment around Er^{3+}. The oscillator strengths of the $^4I_{15/2} \rightarrow {}^4G_{11/2}$ transition of the SGG and SGGC2 samples are 7.092 and 5.993, respectively. Lower oscillator strength in the glass ceramic sample may be due to the higher-inhomogeneity environment in glass compared with $NaYF_4$ NCs in the SGGC2 sample [21].

E. Emission Spectra and Emission Cross Section

As revealed by the structural analysis of glass and glass ceramics, the germanosilicate glass ceramic can provide multiple local structures for RE ions. The local environment of RE ions in such glass ceramics containing complicated structure, in fact, was determined by heat treatment condition. For example, the distribution of RE ions in glass ceramics was affected by heat treatment temperature. The increased heat treatment temperature facilitated the incorporation of RE ions into fluoride NCs, and can make the RE ions distribute in multiple local structures easily. In order to reveal the influence of altering heat treatment temperature on the fluorescence behavior of glass ceramic, upconversion and 2 and 2.7 μm emission spectra were all measured under 980 nm laser diode excitation. As depicted in Fig. 5(a), intense green and red upconversion emissions of Er^{3+} and Ho^{3+} are obtained in glass ceramics while they are weak in glass. The significant enhancement of upconversion emissions from Er^{3+} and Ho^{3+} ions is attributed to the incorporation of Er^{3+} and Ho^{3+} ions into $NaYF_4$ NCs, which provides a low-phonon-energy environment. In addition, a Stark split of 656 nm upconversion emission due to energy level splitting in the crystal field is also observed in all SGGCs while it does not occur in the SGG; this is also observed in other glass ceramic systems [22,23]. The mid-infrared emission spectra in the samples were measured to identify targeted broadening of spectra in germanosilicate glass ceramics. As shown in Fig. 5(b), the full width at half-maximum (FWHM) of the 2 μm emission spectrum is close to 178, 186, 190, and 192 nm for the SGG, SGGC1, SGGC2, and SGGC3 samples, respectively. On the other hand, as shown in Fig. 5(c), the FWHM of the 2.7 μm emission spectrum is close to 140, 164, 154, and 172 nm for the SGG, SGGC1, SGGC2, and SGGC3 samples, respectively.

The results confirm that the broadening of the mid-infrared emission spectra is achieved in the designed glass ceramics. In addition, the intensity of the 2.7 μm emission was enhanced at first, with the increase of heat treatment temperature; however, it decreased when the temperature further increased from 620°C to 640°C. The decreased 2.7 μm emission of Er^{3+} ions was attributed to enhanced upconversion emission of Er^{3+} ions. In this case, the intensity change of the mid-infrared emission of RE ions in low-phonon-energy environment would be related to RE ion concentration. Further, it can be found that the 2.7 μm emission spectrum of the SGG sample is basically a Gaussian peak while the 2.7 μm emission spectra of the SGGC samples have two small bulges at around 2640 and 2800 nm compared with the former, which will be explained in next section. Furthermore, as shown in the inset of Fig. 5(d), the lifetime of $^4I_{11/2}$ level in the SGGC2 sample was as high as 2.51 ms, which is beneficial to obtaining 2.7 μm laser output. Based on these discussions, it can be concluded that the influence of heat treatment temperature on mid-infrared emission in SGGCs is complicated due to the distribution of RE ions in glass ceramics and possibly changed energy transfer. The involved energy transfer will be discussed later.

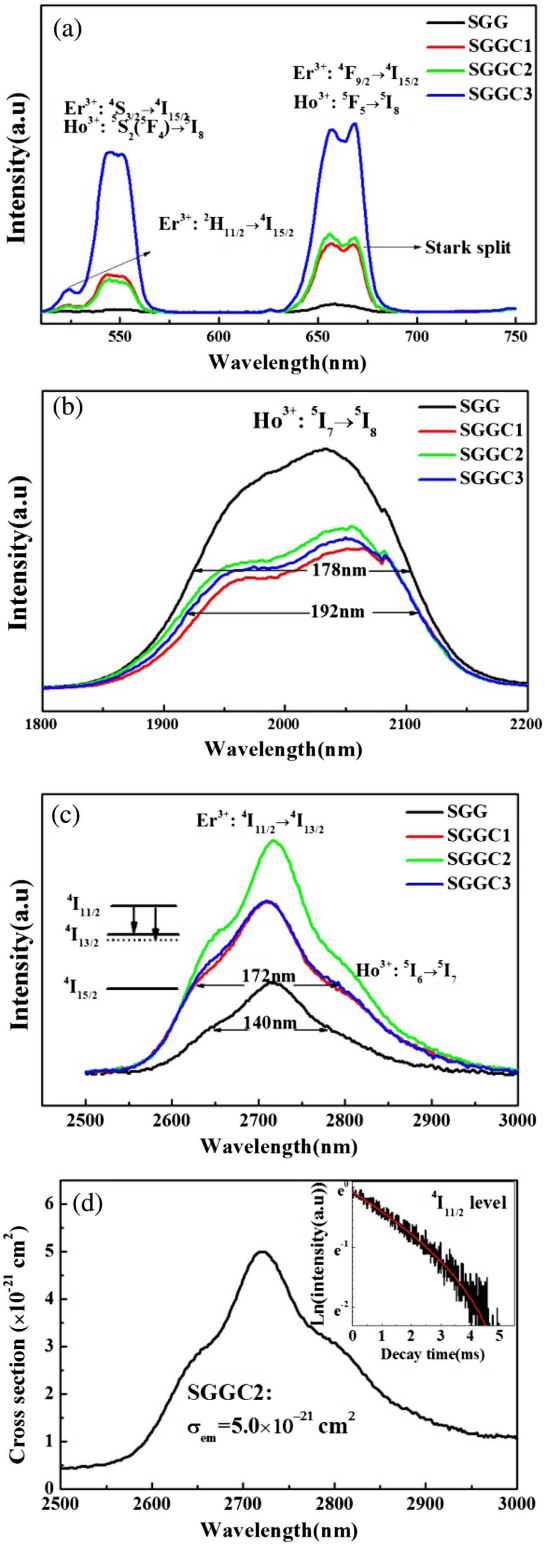

Fig. 5. (a) Visible upconversion emission spectra, (b) 2 μm emission spectra, (c) 2.7 μm emission spectra, and (d) 2.7 μm emission cross section and decay curve of $^4I_{11/2}$ level (inset) in the SGGC2 sample.

To evaluate the potential applications of glass ceramic in mid-infrared host materials, the 2.7 μm emission cross section of the SGGC2 sample was calculated by the Füchtbauer–Ladenburg equation:

$$\sigma_{em}(\lambda) = \frac{\lambda^5 A_{rad}}{8\pi c n^2} \frac{I(\lambda)}{\int \lambda I(\lambda) d(\lambda)}, \quad (1)$$

where λ is the wavelength, $I(\lambda)$ is the fluorescence intensity, and c and n are the light speed and index of refraction (here, the value is 1.532), respectively. The spontaneous radiative transition probability A_{rad} was obtained based on measured absorption spectra and Judd–Ofelt theory [24,25]. In view of the fact that the Er^{3+}:$^4I_{11/2} \rightarrow {}^4I_{13/2}$ transition was much stronger than the Ho^{3+}:$^5I_6 \rightarrow {}^5I_7$ transition in present glass ceramics, the $A_{rad}(22.91\ s^{-1})$) used here is the spontaneous radiative probability of Er^{3+}:$^4I_{11/2} \rightarrow {}^4I_{13/2}$ transition. The calculated result is plotted in Fig. 5(d), and one can find that the peak emission cross section at 2.7 μm is 5.0×10^{-21} cm^2, which is comparable to Er^{3+}-doped ZBLAN glass (5.7×10^{-21} cm^2) [26]. Combined with the high emission cross section and broadband spectra at 2.7 μm, oxyfluoride germanosilicate glass ceramic may be a promising and competitive candidate for mid-infrared tunable laser host materials.

F. Energy Transfer Mechanism

The more complicated glass network in glass ceramic creates a range of dipole environments, which may explain the broadening of the 2 μm emission spectra. However, there are more reasons for the change in 2.7 μm emission spectra in SGGCs. Understanding the energy transfer mechanism of RE ions is beneficial to comprehending the reason for enhancing and broadening the 2.7 μm emission in SGGCs. On the basis of measured emission spectra and previous reports [8,27,28], an energy-level diagram of Er^{3+} and Ho^{3+} is depicted in Fig. 6 and the energy transfer mechanism of Er^{3+} and Ho^{3+} ions is proposed as follows.

First, the ions at the ground state Er^{3+}:$^4I_{15/2}$ level absorb energy from the pump source (980 nm LD) and are excited to the $^4I_{11/2}$ level.

On one hand, the ions at the Er^{3+}:$^4I_{11/2}$ level can not only transfer energy to the Ho^{3+}:$^5I_6$ level (ET1:Er^{3+}:$^4I_{11/2}$ + Ho^{3+}:$^5I_8 \rightarrow Ho^{3+}$:$^5I_6 + Er^{3+}$:$^4I_{15/2}$), but they can also decay to the Er^{3+}:$^4I_{13/2}$ level by nonradiative decay or radiative transition (Er^{3+}:$^4I_{11/2} \rightarrow Er^{3+}$:$^4I_{13/2}$ + 2.7 μm). Then, the ions at the Er^{3+}:$^4I_{13/2}$ level can transfer energy to the Ho^{3+}:$^5I_7$ level (ET2:Er^{3+}:$^4I_{13/2} + Ho^{3+}$:$^5I_8 \rightarrow Ho^{3+}$:$^5I_7 + Er^{3+}$:$^4I_{15/2}$) due to small energy gap between them. The ions at the Ho^{3+}:$^5I_7$ level can radiate energy to the ground state Ho^{3+}:$^5I_8$ level, generating 2 μm light emission.

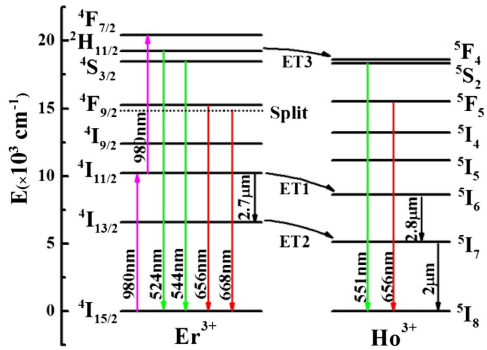

Fig. 6. Energy level diagrams and energy transfer mechanism from Er^{3+} to Ho^{3+}.

On the other hand, the ions at the Er^{3+}:$^4I_{11/2}$ level can reabsorb 980 nm photon energy and are excited to a higher Er^{3+}:$^4F_{7/2}$ level, which nonradiatively decays subsequently to lower excited energy levels. The ions at the excited energy levels of Er^{3+} can not only transfer energy to adjacent excited energy levels of Ho^{3+} (i.e., ET3:Er^{3+}:$^2H_{11/2}$ + Ho^{3+}:$^5I_8 \rightarrow Ho^{3+}$:$^5F_4$ + Er^{3+}:$^4I_{15/2}$), but they can also radiate their energy to the ground state Er^{3+}:$^4I_{15/2}$ level, generating upconversion emissions (i.e., 524, 544, 656, 668 nm, etc.). Similarly, the ions at the excited energy levels of Ho^{3+} can generate light emissions (i.e., 551, 656 nm, etc.) by radiative transition. The ions at the Er^{3+}:$^4I_{11/2}$ level easily decay nonradiatively to lower levels in high phonon energy environments, and therefore the energy transfer processes mentioned in this paragraph mainly happen in $NaYF_4$ NCs.

Thus, we can conclude that the 668 nm emission in glass ceramics originates from the transition between the splitting energy level of Er^{3+}:$^4F_{9/2}$ and the ground state Er^{3+}:$^4I_{15/2}$ level. In addition, the change in peak shape of 2.7 μm spectra can be attributed to the energy level splitting of Er^{3+} in the crystal field (bulge at 2640 nm) and the enhancement of Ho^{3+}:$^5I_6 \rightarrow {}^5I_7$ transition (bulge at 2800 nm). It is noted that the energy level splitting of Er^{3+}:$^4I_{13/2}$ reflected in the 2.7 μm emission spectra has a good agreement with the results of the absorption spectra, as shown in the inset of Figs. 4(b) and 5(c). However, the origins of decreased 2 μm emission and enhanced 2.8 μm emission of Ho^{3+} in glass ceramic are still unclear, which can be revealed by further non-resonant energy transfer analysis between Er^{3+} and Ho^{3+} in the next section.

G. Non-Resonant Energy Transfer Analysis

In order to broaden the mid-infrared spectra around 2.7 μm, it is necessary for Er^{3+} to transfer some energy to Ho^{3+}, which can generate 2.8 μm (close to 2.7 μm) emission through $^5I_6 \rightarrow {}^5I_7$ radiative transition. Although the SGG sample with high phonon energy can promote energy transfer from Er^{3+} to Ho^{3+} with the assistance of fewer phonons, it also leads to high multi-phonon relaxation rates and weakens the mid-infrared emissions. Hence, it is necessary to quantitatively investigate the energy transfer process further, which can be evaluated by the calculations of the absorption and emission cross sections of Er^{3+} and Ho^{3+} ions using Dexter theory [29]. When phonon assistance is taken into consideration, the Dexter expression for the energy transfer coefficient (C_{DA}) by dipole–dipole mechanism can be expressed as

$$C_{DA} = \frac{6cg_{low}^D}{(2\pi)^4 n^2 g_{up}^D} \sum_{m=0}^{\infty} e^{-(2\bar{n}+1)S_0} \frac{S_0^m}{m!} (\bar{n}+1)^m \times \int \sigma_{ems}^D(\lambda_m^+) \sigma_{abs}^A(\lambda) d(\lambda), \quad (2)$$

where c is the light speed in vacuum, n is the refractive index of the medium, and g_{low}^D and g_{up}^D are the degeneracy of the lower and upper levels of the donor (here, Er^{3+}), respectively. $\hbar\omega_0$ is

the maximum phonon energy (here, 1050 and 300 cm^{-1} were used for glass and $NaYF_4$ NCs, respectively) [30], $\bar{n}$ is the average occupancy, m is the number of phonons participating in the energy transfer, S_0 is the Huang–Rhys factor (0.31 for RE ions), and $\lambda_m^+ = 1/(1/\lambda - m\hbar\omega_0)$ is the wavelength with m phonon creation. In the SGGC2 sample, C_{DA} is calculated for rare earth ions distributed both in glass and $NaYF_4$ NCs.

The absorption and emission cross sections of Er^{3+} and Ho^{3+} ions in the SGG and SGGC2 samples are calculated based on measured absorption spectra and the McCumber formula [31], which are presented in Fig. 7. It can be seen that emission cross section of Er^{3+} does not overlap with the absorption cross section of Ho^{3+} in both glass and glass ceramic samples. Therefore, phonons are required to assist energy transfer from Er^{3+} to Ho^{3+} ions in both the ET1 and ET2 processes.

For the ET2 process, three or four phonons are needed to fill the energy gap between Er^{3+}:$^4I_{13/2} \rightarrow Er^{3+}$:$^4I_{15/2}$ emission and Ho^{3+}:$^5I_8 \rightarrow Er^{3+}$:$^5I_7$ absorption in $NaYF_4$ NCs. However, only one phonon is required for the ET2 process in glass. The calculation results also show that the C_{DA} of the ET2 process is 1.88×10^{-41} cm^2 in $NaYF_4$ NCs embedded in SGGC2 sample, significantly lower than that in SGG sample (11.75×10^{-41} cm^2) and SGGC2 glass matrix (10.08×10^{-41} cm^2). These results indicate that the ET2 process is more efficient in germanosilicate glass than in $NaYF_4$ NCs, which can explain the decrease of 2 μm emission in glass ceramic.

For the ET1 process, three or four phonons are also needed to fill the energy gap between Er^{3+}:$^4I_{11/2} \rightarrow Er^{3+}$:$^4I_{15/2}$ emission and Ho^{3+}:$^5I_8 \rightarrow Er^{3+}$:$^5I_6$ absorption in $NaYF_4$ NCs. However, only one phonon is required for the ET1 process in glass. The calculation results also show that the C_{DA} of the ET1 process is 0.44×10^{-41} cm^2 in $NaYF_4$ NCs embedded in SGGC2 sample, significantly lower than that in SGG sample (1.10×10^{-41} cm^2) and SGGC2 glass matrix (1.25×10^{-41} cm^2). These results indicate that the ET2 process is stronger than the ET1 process for energy transfer between Er^{3+} and Ho^{3+}. What's more, the results also indicate that the enhanced 2.8 μm emission in glass ceramic originates from the enhancement of energy transfer between higher energy levels of Er^{3+} and Ho^{3+} (i.e., ET3:Er^{3+}:$^2H_{11/2}$ + Ho^{3+}:$^5I_8 \rightarrow Ho^{3+}$:$^5F_4$ + Er^{3+}:$^4I_{15/2}$) rather than the enhancement of the ET1 process.

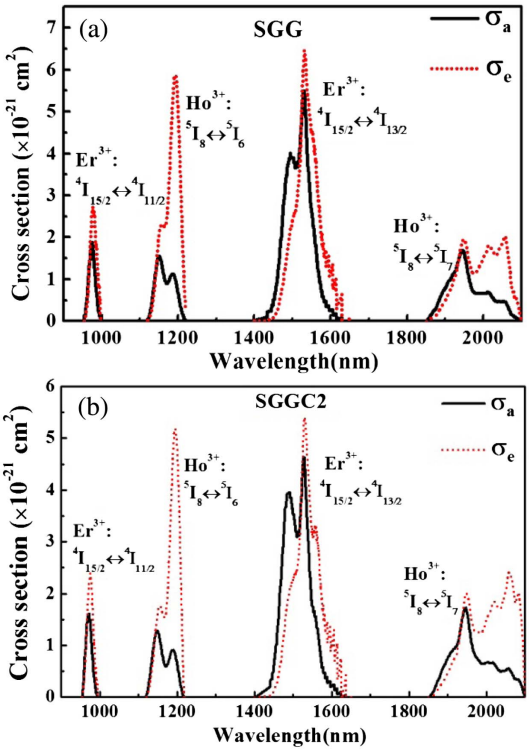

Fig. 7. Absorption and emission cross sections of Er^{3+} and Ho^{3+} in (a) SGG glass and (b) SGGC2 sample.

4. CONCLUSION

In summary, Er/Ho co-doped oxyfluoride germanosilicate glass and glass ceramic containing $NaYF_4$ NCs were prepared. Differential thermal analysis indicates the germanosilicate glass has good thermal stability. Transmission electron microscopy and X-ray diffraction demonstrate that both the formation of $NaYF_4$ NCs during the heat treatment processes and the increase of heat treatment temperature can accelerate the growth of $NaYF_4$ NCs, together with the incorporation of more RE ions. The glass network consists of SiO_4 and GeO_4 structural units, while the network of the glass ceramics consists of SiO_4, GeO_4, and GeO_6 units together with $NaYF_4$ NCs. Therefore, RE ions can locate at multiple local structures in oxyfluoride germanosilicate glass ceramics.

Absorption spectra were measured and the results indicate that the formation of $NaYF_4$ NCs has an influence on the hypersensitive transitions and $^4I_{13/2} \rightarrow {}^4I_{15/2}$ absorption of Er^{3+} ions. Upconversion emissions were significantly enhanced, and Stark split of green emission occurred in glass ceramic samples. Broadening of 2 and 2.7 μm emission spectra, together with the change in spectra shape, were observed in oxyfluoride germanosilicate glass ceramics. Analyses were conducted of the energy transfer mechanism between Er^{3+} and Ho^{3+} and the non-resonant energy transfer to comprehend the change in fluorescence spectra. The results indicate that the reasons for the broadening of the 2.7 μm emission spectra in SGGCs are: (1) more complicated glass network, (2) energy level splitting of Er^{3+} in crystal field, and (3) the enhancement of Ho^{3+}:$^5I_6 \rightarrow {}^5I_7$ transition in $NaYF_4$ nanocrystals. The calculation of C_{DA} for the ET2 process can explain the decreased 2 μm emission and indicate the origin of enhanced 2.8 μm emission in glass ceramics.

Funding. National Natural Science Foundation of China (NSFC) (51472225, 61775205, 51372236, 61605192); Natural Science Foundation of Zhejiang Province (LD18F050001).

REFERENCES

1. Y. Tsang, B. Richards, D. Binks, J. Lousteau, and A. Jha, "Tm^{3+}/Ho^{3+} codoped tellurite fiber laser," Opt. Lett. **33**, 1282–1284 (2008).
2. T. Hu, B. Dong, X. Luo, T.-Y. Liow, J. Song, C. Lee, and G.-Q. Lo, "Silicon photonic platforms for mid-infrared applications [Invited]," Photon. Res. **5**, 417–430 (2017).
3. M. Klimczak, B. Siwicki, A. Heidt, and R. Buczyński, "Coherent supercontinuum generation in soft glass photonic crystal fibers," Photon. Res. **5**, 710–727 (2017).

4. C. R. Petersen, U. Møller, I. Kubat, B. Zhou, S. Dupont, J. Ramsay, T. Benson, S. Sujecki, N. Abdel-Moneim, Z. Tang, D. Furniss, A. Seddon, and O. Bang, "Mid-infrared supercontinuum covering the 1.4-13.3 μm molecular fingerprint region using ultra-high NA chalcogenide step-index fibre," Nat. Photonics **8**, 830–834 (2014).
5. W. J. Chung, K. H. Kim, B. J. Park, H. S. Seo, J. T. Ahn, and Y. G. Choi, "Radiative emission at mid-infrared wavelengths from rare-earth ions via nanocrystal formation in oxyfluoride glasses," J. Am. Ceram. Soc. **93**, 2952–2955 (2010).
6. R. Xu, Y. Tian, L. Hu, and J. Zhang, "Enhanced emission of 2.7 μm pumped by laser diode from Er^{3+}/Pr^{3+}-codoped germanate glasses," Opt. Lett. **36**, 1173–1175 (2011).
7. A. Lin, A. Ryasnyanskiy, and J. Toulouse, "Fabrication and characterization of a water-free mid-infrared fluorotellurite glass," Opt. Lett. **36**, 740–742 (2011).
8. Y. Tian, T. Wei, X. Jing, J. Zhang, and X. Xu, "Enhanced 2.7- and 2.9-μm emissions in Er^{3+}/Ho^{3+}, doped fluoride glasses sensitized by Pr^{3+} ions," Mater. Res. Bull. **76**, 67–71 (2016).
9. P. P. Fedorov, A. A. Luginina, and A. I. Popov, "Transparent oxyfluoride glass ceramics," J. Fluorine Chem. **172**, 22–50 (2015).
10. G. Bai, S. Yuan, Y. Zhao, Z. Yang, S. Y. Choi, Y. Chai, S. F. Yu, S. P. Lau, and J. Hao, "2D layered materials of rare-earth Er-doped MoS_2 with NIR-to-NIR down- and up-conversion photoluminescence," Adv. Mater. **28**, 7472–7477 (2016).
11. G. Bai, M.-K. Tsang, and J. Hao, "Luminescent ions in advanced composite materials for multifunctional applications," Adv. Funct. Mater. **26**, 6330–6350 (2016).
12. Q. Liu, Y. Tian, C. Wang, F. Huang, X. Jing, J. Zhang, X. Zhang, and S. Xu, "Different dominant transitions in holmium and ytterbium codoped oxyfluoride glass and glass ceramics originating from varying phonon energy environments," Phys. Chem. Chem. Phys. **19**, 29833–29839 (2017).
13. V. Lupei, "Laser materials: relationship between materials and laser properties," in *Reference Module in Materials Science and Materials Engineering* (2016), pp. 4416–4423.
14. A. Jha, B. Richards, G. Jose, T. Teddy-Fernandez, P. Joshi, X. Jiang, and J. Lousteau, "Rare-earth ion doped TeO_2 and GeO_2 glasses as laser materials," Prog. Mater. Sci. **57**, 1426–1491 (2012).
15. Q. Liu, Y. Tian, B. Li, C. Wang, F. Huang, X. Jing, J. Zhang, and S. Xu, "Broadband 2 μm fluorescence and energy transfer process in Tm^{3+} doped germanosilicate glass," J. Lumin. **190**, 76–80 (2017).
16. Q. Chen, H. Wang, Q. Wang, and Q. Chen, "Structural study of the origin of the largest 1.5 μm Er^{3+} luminescence band width in multicomponent silicate glass," J. Non-Cryst. Solids **404**, 145–150 (2014).
17. J. Kimpton, T. H. Randle, and J. Drennan, "Investigation of electrical conductivity as a function of dopant-ion radius in the systems $Zr_{0.75}Ce_{0.08}M_{0.17}O_{1.92}$ (M = Nd, Sm, Gd, Dy, Ho, Y, Er, Yb, Sc)," Solid State Ionics **149**, 89–98 (2002).
18. H. A. Elbatal, Z. S. Mandouh, H. A. Zayed, S. Y. Marzouk, G. M. Elkomy, and A. Hosny, "Thermal, structure and morphological properties of lithium disilicate glasses doped with copper oxide and their glass-ceramic derivatives," J. Non-Cryst. Solids **358**, 1806–1813 (2012).
19. D. Di Martino, L. F. Santos, A. C. Marques, and R. M. Almeida, "Vibrational spectra and structure of alkali germanate glasses," J. Non-Cryst. Solids **293-295**, 394–401 (2001).
20. P. Pascuta, L. Pop, S. Rada, M. Bosca, and E. Culea, "The local structure of bismuth germanate glasses and glass ceramics doped with europium ions evidenced by FT-IR spectroscopy," Vib. Spectrosc. **48**, 281–284 (2008).
21. L. R. Moorthy, T. S. Rao, K. Janardhnam, and A. Radhapathy, "Absorption and emission characteristics of Er^{3+} ions in alkali chloroborophosphate glasses," Spectrochim. Acta A **56**, 1759–1771 (2000).
22. X. Qiao, X. Fan, M. Wang, and X. Zhang, "Spectroscopic properties of Er^{3+}–Yb^{3+} co-doped glass ceramics containing BaF_2 nanocrystals," J. Non-Cryst. Solids **354**, 3273–3277 (2008).
23. F. Zeng, G. Ren, X. Qiu, Q. Yang, and J. Chen, "The effect of PbF_2 content on the microstructure and upconversion luminescence of Er^{3+}-doped SiO_2–PbF_2–PbO glass ceramics," J. Non-Cryst. Solids **354**, 3428–3432 (2008).
24. B. R. Judd, "Optical absorption intensities of rare-earth ions," Phys. Rev. **127**, 750–761 (1962).
25. G. S. Ofelt, "Intensities of crystal spectra of rare-earth ions," J. Chem. Phys. **37**, 511–520 (1962).
26. Y. Tian, R. Xu, L. Hu, and J. Zhang, "Intense 2.7 μm and broadband 2.0 μm emission from diode-pumped Er^{3+}/Tm^{3+}/Ho^{3+}-doped fluorophosphate glass," Opt. Lett. **36**, 3218–3220 (2011).
27. T. Wei, C. Tian, M. Cai, Y. Tian, X. Jing, J. Zhang, and S. Xu, "Broadband 2 μm fluorescence and energy transfer evaluation in Ho^{3+}/Er^{3+} codoped germanosilicate glass," J. Quantum Spectrosc. Radiat. Transfer **161**, 95–104 (2015).
28. T. Wei, Y. Tian, C. Tian, M. Cai, X. Jing, B. Li, R. Chen, J. Zhang, and S. Xu, "Quantitative analysis of energy transfer and origin of quenching in Er^{3+}/Ho^{3+} codoped germanosilicate glasses," J. Phys. Chem. A **119**, 6823–6830 (2015).
29. D. L. Dexter, "A theory of sensitized luminescence in solids," J. Chem. Phys. **21**, 836–850 (1953).
30. A. D. Sontakke and K. Annapurna, "Energy transfer kinetics in oxy-fluoride glass and glass-ceramics doped with rare-earth ions," J. Appl. Phys. **112**, 013510 (2012).
31. D. E. McCumber, "Theory of phonon terminated optical lasers," Phys. Rev. **134**, A299–A306 (1964).